A TRAVERSABLE FLOW PROBE TO MEASURE LAMINAR BOUNDARY LAYER PROPERTIES OVER SUCTION SKINS

K. Alt*, K. Thamm†*, M. Corelli Grappadelli†*, R. von Soldenhoff†‡, H. Lüdeke‡†, P. Scholz*†
† Exzellenzcluster SE²A – Sustainable and Energy-Efficient Aviation, TU Braunschweig
* Technische Universität Braunschweig – Institut für Strömungsmechanik, Braunschweig
‡ Deutsches Zentrum für Luft- und Raumfahrt - Institut für Aerodynamik und Strömungstechnik, Braunschweig

Abstract

A traverseable flow probe was developed to measure boundary layer data for laminar boundary layers over suction skins. Boundary layer data is a key to verify transition predictions and to exactly trace the development of instabilities in laminar boundary layers. Measurement of boundary layer data is particularly intricate over micro-porous surfaces used for laminar flow control, because any probe must me mounted well downstream of the suction area. The probe presented herein can traverse a single-element hot-wire in, both, streamwise and wall-normal direction over distances of 365 mm and 52 mm, respectively, with a stiffness and accuracy making it suitable to measure velocity profiles of boundary layers, but also amplitude functions of Tollmien-Schlichting waves. The probe is modular and can be used in two different large-scale experimental setups with flat plates. Some boundary layer profiles, including suction for laminar flow control, will be shown taken from an entry in the wind tunnel MUB.

Keywords

Laminar Flow Control; Boundary Layer Suction; Laminar Boundary Layer

1. INTRODUCTION

Boundary layer suction for laminar flow control (LFC) is known for decades, but has not yet played a major role for current aircraft design. For future transport aircraft, however, assuming that fuel consumption and environmental impact will become the driving factor, boundary layer suction could deliver significant contributions in reducing the drag and thus the fuel burn during flight.

Boundary layer suction has been studied extensively for airfoils [1], [2], ranging from sailplane applications [3] to transonic airfoil design [4] and also in the form of hybrid laminar flow control (HLFC), e.g. [5], [6] and many others.

Though the majority of more applied studies focuses on laminar wings or airfoils, LFC can probably be very efficient on the fuselage of an aircraft, because the boundary layer experiences only weak pressure gradients. The stability is dominated by Tollmien-Schlichting-waves (TS-waves) and, more specifically, viscous modes of TS-waves in boundary layers with large characteristic Reynolds numbers. For fundamental research in this field, flat plates can be used in wind tunnels. E.g. Lüdeke & Breitenstein [7] started investigations on concepts to keep the boundary layer laminar over long distances on a flat plate. Hildebrand et al. [8] and Scholz et al. [9] took in consideration, how local instabilities, e.g. steps, effect the behavior of a laminar boundary layer and trigger laminar-turbulent transition in downstream direction.

Several methods, most often based on linear local stability theory, can serve to predict transition for given pressure distributions. Corelli Grappadlli et al. [10] used a flat plate with zero pressure gradient to compare the prediction of the transition position based on the e^N-method, with wind tunnel data, including the effect of suction. The results show, that the transition position moves downstream if suction rate increases, but when exceeding some optimum value an adverse trend occurs. Also several other studies have recognized that too strong suction is decreasing efficiency. The reasons may be very diverse, e.g. the suction through the discrete suction holes may create some aerodynamic roughness. Also, the impedance of the suction system (particularly the skin and the underlying manifold) may play a role, [11]. Furthermore, most studies focus on measuring the pressure distribution and the transition position and then compare the results to some predictions (e.g. e^N-method), ultimately aiming e.g. to quantify a more-or-less constant $N_{crit.}$ for the suction cases. This approach features quite some uncertainties, [12], e.g. only the integral suction muss flow is usually known, the boundary layer prediction relies on more-or-less simplified boundary conditions and the amplification factors are a sensible result of the predictions of the laminar boundary layer profiles.

To gain more insight, more detailed data about the boundary layer must be measured, which is typically done by the means of (traversing) probes, [13], [14]. Design of such probes can be an intriguing task. Probes traversing in wall-normal direction can already become complex little devices, since – even on large flat plates – the boundary layer thickness of the laminar boundary layers is only a few millimeters. To make the best use out of limited wind tunnel time, it is even more desirable to have a probe that can also traverse in streamwise direction, such that not only local boundary layer profiles can be measured, but also their development. In the cluster of excellence "sustainable and energy efficient aviation" (SE²A) the institute of fluid mechanics (ISM) at TU Braunschweig and the institute of aerodynamics and flow technology (DLR/AS) of DLR Braunschweig share a project about the measurement of suction boundary layers on large flat plates. In this project, a traversable probe is desired, which can traverse in, both, streamwise and wall-normal direction and which can be used in a modular way in two different experimental environments: For one in the flat plate setup at ISM, which was ultimately developed by Corelli Grappadelli et al. [10] for the wind tunnel "MUB"

doi: 10.25967/610146

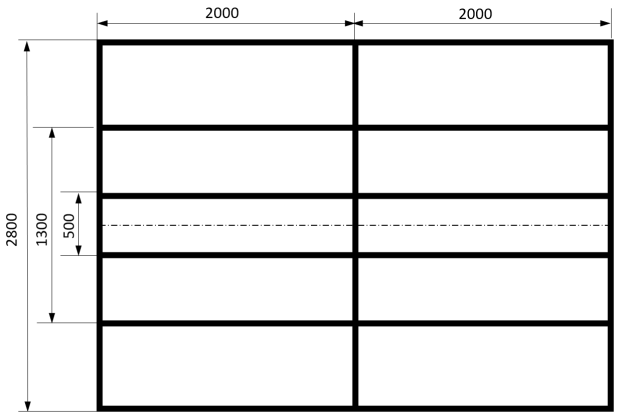

FIG 1. ITEM frame of the flat plate model at the DNW-NWB

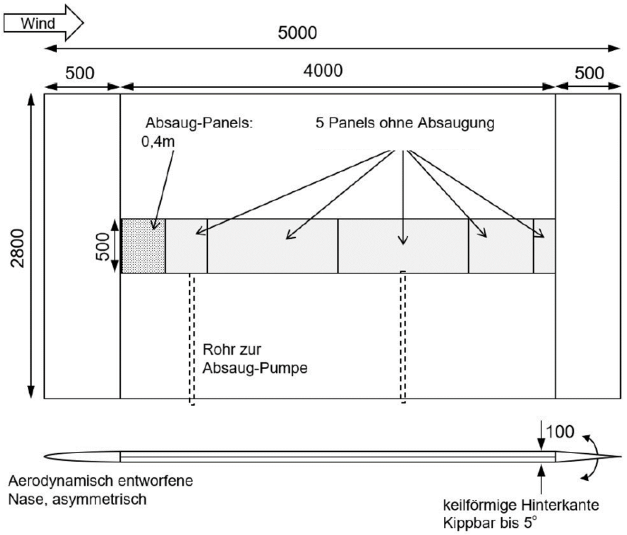

FIG 2. Modular design of the flat plate at the DNW-NWB [15]

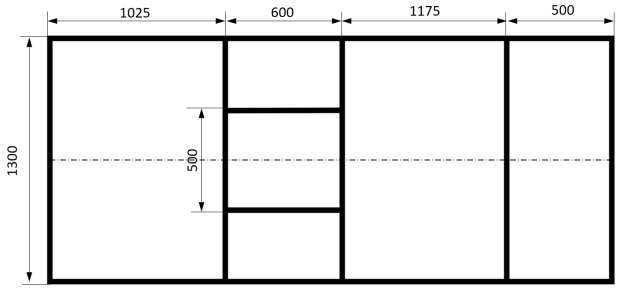

FIG 3. ITEM frame of the flat plate model for wind tunnel MUB

at ISM. The same probe shall also be used for the very large flat plate setup for the wind tunnel "NWB", which is described in [7].
Herein, the design of the probe and results of an initial experimental entry in the wind tunnel "MUB" at ISM will be presented. The test cases used in the entry, in terms of flow velocities, Reynolds number and suction rates, are taken from Corelli Grappadelli et al. [10].

2. WIND TUNNELS AND METHODOLOGY

The traversable hot-wire probe will be used in different wind tunnel entries in two different wind tunnels. Therefore, in this section the two different wind tunnel setups are described to explain the general dimensions. Also, continuously the data will be compared to results of a boundary layer prediction and linear local stability analysis. The tools used will also briefly be addressed.

2.1. Wind tunnel DNW-NWB

The "Niedergeschwindigkeits-Windkanal Braunschweig" (NWB) is operated by the Deutsch-Niederländische Windkanäle (DNW). The DNW-NWB is a subsonic wind tunnel of Göttingen design and has a closed test section of 8m length. The rectangular test section is 3.25m in width and 2.80m in height. The test section is modular and can be operated as a closed section, a slotted section and also in a open jet configuration. However, herein only the closed setup was used, for which the tunnel can operate up to 90 m/s.
The flat plate model is placed vertically in the test section. The basic structure of the model, shown in Fig. 1, is made out of aluminum construction profiles ("ITEM"-profiles, where ITEM is a German manufacturer). The length of the flat plate is 5 m, the thickness is 0.1 m, the span is 2.8 m. The panels mounted on the profiles are modular. The typical configuration of the modular surface panels is shown in Fig. 2. The aerodynamically designed asymmetric nose and the wedge-shaped trailing edge of the flat plate both have a chord of 0.5 m. The trailing edge is basically a flap, which can rotate by ±5° to adjust the exact position of the stagnation point on the leading edge. All surface panels are 8.8 mm thick and the underlying ITEM profiles have dimensions of 40x80 mm². Thus, there is free space of 80 mm thickness between the panels on both sides of the frame, which can house the traversing probe.
Due to the modularity, the surface panels can be arranged with great freedom. Only the general setup of the ITEM profiles, as shown in figure 1, must be held constant for structural reasons. The core element of the flat plate model is the 0.4 m suction panel, which is integrated directly downstream of the leading edge module, as shown in Fig. 2. The suction panel has a chord length of 0.4 m. Therefore, when the traverse is installed directly downstream of the suction panel, to gather boundary layer profiles along the whole suction surface a traversing distance of 0.4 m in chordwise direction is required.
Note that, although the traverse is being designed to be used in this setup, herein we will not discuss results from DNW-NWB.

2.2. Wind Tunnel MUB

The "Modell Unterschallwindkanal Braunschweig" MUB is located at the Institut für Strömungsmechanik (ISM) at TU Braunschweig. It is a modular tunnel and the test section can be configured to host various different experimental setups. The larger test section, which was used herein, has a length of 5.0 m and a square cross-section with a length of 1.3m. The MUB can operate up to 60 m/s for this test section.
Very similar to the NWB flat plate model, the basic backbone of the MUB flat plate model is built from ITEM-type aluminum construction profiles and thus also has a modular structure that is shown in Fig. 3. The leading edge of the plate model is symmetrical and was specifically designed to generate a smooth pressure distribution for laminar boundary layers, [10], by limiting the suction peak and thus avoiding early growth of instabilities. The suction panel is located just downstream of the leading edge section and covers $x/c = 0.17$ to $x/c = 0.28$. It basically consists of a suc-

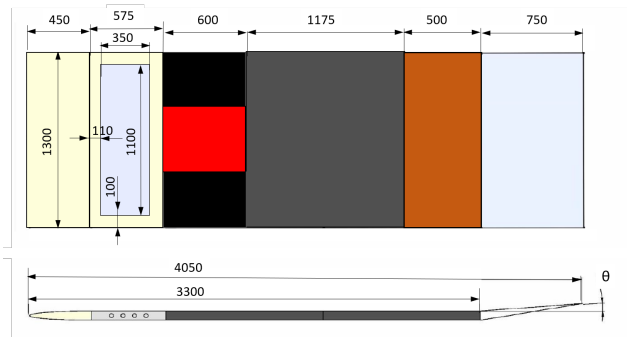

FIG 4. Modular design of the flat plate model for wind tunnel MUB

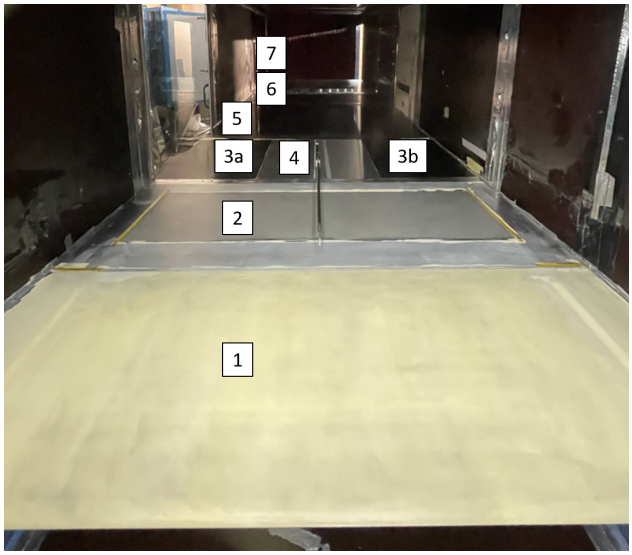

FIG 5. Installed flat plate with hot-wire traverse, seen from the leading edge looking in downstream direction

tion box and a porous surface bonded to it, shown in Fig. 4. The suction surface used in this setup is a laser drilled surface with holes of 120 µm diameter and a porosity of 0.01. The traversable probe was placed in the surface panel just downstream of the suction panel. In this case, just as for the NWB-setup, to cover the whole suction panel the traverse must cover a distance of 0.4 m in chordwise direction.
The flat plate model is instrumented with a number of static pressure taps, which are located in the side regions of the plate, 160 mm from the wind tunnel walls to avoid any disturbances in the center section. Herein, only the boundary layer upstream of the traverse is of interest, therefore pressure was measured only along the first 30 % of the flat plate. A total of 28 pressure taps exist on each side of the plate, 22 of which are relevant for the suction side flow. The taps have a diameter of 0.3mm. Reference conditions are measured with a pitot-static-combination (Prandtl probe) well above the plate. For each data point, 2500 samples are recorded at 20 Hz and then averaged to calculate the pressure coefficient.
Since the traverse will disturb the flow it is generally not possible to measure the boundary layer profiles with the traverse and the transition position (with thermal imaging) at the same time. Only a sequential operation is possible. In the study discussed herein, thermal imaging was not done. Instead, all cases are based on results of the same experiment published by Corelli Grapedelli et al. [10], where transition position is given for several different flow velocities (or Re, respectively) and several different suction rates.

An image of the traverse finally implemented into the flat plate model of Corelli [10] is shown in Fig. 5. For the plate assembly, the ITEM profile structure and the nose (1) were first aligned and mounted in the wind tunnel 450mm above the wind tunnel floor. Then, the adjustable trailing edge flap (7) was fixed directly to the wind tunnel wall. The deflection of the flap is -4°. The suction panel (2), the traversing hot-wire probe (4), the glass-fiber reinforced plastic (FRP) panels (3a and 3b), a fiber composite panel (5) and two screen-printed panels (6) were mounted on the ITEM section structure from front to back.
The traversing probe panel (4) and the FRP panels to the right and left of it, (3a) and (3b), were mounted on the ITEM profile structure using multiblocks manufactured by ITEM. The multiblocks allow the panels to be adjusted step by step in relation to each other.

2.3. Boundary layer prediction and linear stability analysis

The boundary layer profiles and instabilities measured with the traversing hot-wire probe will be compared to predictions based on analytical/numerical tools. The tool chain used herein is the combination of the boundary layer solver COCO (*COmpressible, COnical boundary layer solver*) [16] with the *LInear LOcal stability analysis* method LILO, [17].
The pressure distribution measured in the actual setup is used as an input to COCO. In this step, smoothing and interpolation of additional points is required, which will not be detailed herein. The refined pressure distribution is then used in COCO to predict the boundary layer development, including local boundary layer profiles. COCO solves the laminar, conical boundary layer equations with a finite difference scheme. To generate high-resolution boundary layer profiles, 200 points were used in wall normal direction.
The boundary layer profiles (including derivatives and temperature profiles) from COCO are then fed into LILO, which solves the linear, local stability equations based on the velocities, pressure and Temperature profiles and their derivatives based on a second-order accurate discretization. This forms a generalized eigenvalue problem, which is solved with the temporal approach. The outcome of LILO is disturbance profiles (i.e. amplitude functions) for several different modes and their respective amplification rates.
COCO and LILO in- and outputs are–although they are standalone codes–highly adapted to each other to allow a seamless work flow. COCO/LILO also feature transformation of temporal amplification rates into spatial amplification and integration of spatial amplification, such that finally a full e^N-method is available.

3. HOT-WIRE TRAVERSE

3.1. Hardware

The integration of the hot-wire traverse into the flat plate models uses a metal plate as a base on which the traverse components are placed. This plate fits the ITEM frame dimensions of both wind tunnel models. The traverse is able to move in the x-direction as well as in the wall-normal y-direction. Figure 6 shows an overview of all the components installed on the metal plate. The main element sits on two rails that allow the core to slide in the x-direction, driven by a *NEMA 23* stepper motor. This stepper motor is connected to a ball screw via a belt transmission, which moves a ball nut, as can be seen in Figure 7. End switches on either side

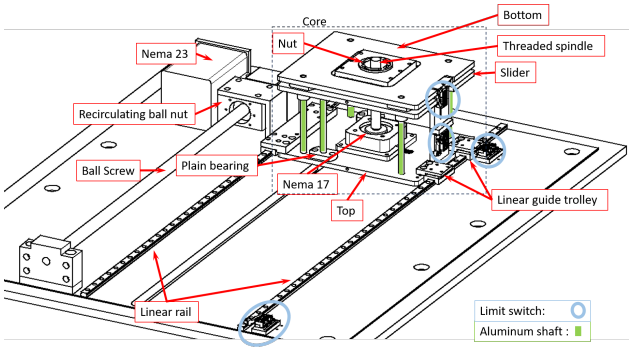

FIG 6. Drawing of the traversable hot-wire probe (lower side)

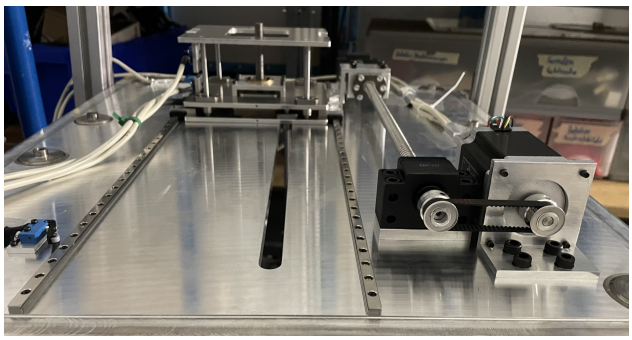

FIG 7. Belt transmission for the x-axis mobility in front right

prevent a collision between the ball nut and the bearings of the spindle and at the same time they allow a referencing of the traverse position.
The current version of the traverse can travel a distance of 365 mm in x-direction, i.e. in flow direction. It is yet limited by the size of the base metal plate (600 mm), which was chosen to fit into the existing paneling of the DNW-NWB-setup. Still, the traverse can reach most of the 400mm suction panel.
The main element of the traverse is basically a well-mounted platform that can be moved in the wall-normal direction. It consists of two plates which support four bearing rods and a spindle. The upper plate also holds a slim (20 mm) *NEMA 17* stepper motor which rotates a fine thread spindle which then moves the "slide platform" in a lateral direction. The hot-wire probe holder assembly is then mounted on this slide platform. The total reach of the slider platform and the hot-wire probe is 52 mm. It is therefore able to move through the entire boundary layer in most cases. Again, end switches on either side prevent a collision between the slider platform and the two plates and at the same time they (should theoretically) allow a referencing of the traverse position.
Two rods protrude through a slit in the baseplate into the boundary layer flow. They hold a 500 mm long pullwinded carbon tube and a 3D-printed angle-piece, which finally holds the off-the-shelve Dantec hot-wire probe holder and the hot-wire itself. In Fig. 8 the arm that holds the hot-wire

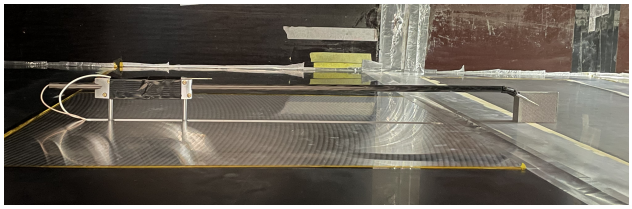

FIG 8. Upper surface of the traverse installed inside the MUB

probe above the upper surface of the metal plate is shown installed in the wind tunnel MUB.
The overall design of the traverse, including the conceptual and structural design, was the key element of a student thesis, [18]. The majority of the elements are either off-the-shelf or based on semi-finished sheet materials to allow efficient fabrication.
For boundary layer traverses, the calibration of the probe head position (i.e. the actual measurement position in wall-normal direction) is very critical and at the same time quite intricate. For the traverse used herein, the end switches should theoretically give a reference position. However, the position of the actual probe head relative to the flat plate surface changes e.g. with even very slight misalignment of the probe support plate or e.g. because the suction surface may bend by some sub-mm with different suction rates. Herein, for a first rough approach the probe head has been imaged by a camera relative to a calibration grid that was put on the plate surface. By post-processing of the images the position can be found with an accuracy of between 0.5 mm and 1 mm. This is certainly not satisfactory. For the preliminary set of data discussed in the present publication the data was corrected regarding the wall-normal position straightforward by fitting it to the COCO-results. In a further development step some method to constantly measure and track the distance between the hot-wire and the flat plate surface is required, e.g. based on miniature distance sensors, and will be implemented for future measurements.

3.2. Hot-wire setup and Data Acquisition

The whole hot-wire setup is basically a commercial off-the-shelve system from Dantec Dynamics, consisting of type 55P11 miniature wire probes, a 55H20 probe support and a Streamline Pro CTA mainframe with a type 9091C0101 CTA module. The system is operated with the dedicated software according to the operation manual, i.e. all bridge balancing and dynamics adjustment is made. The response time of the setup is around 33 kHz and, thus, well larger than any expected TS wave.
The voltage output of the StramlinePro-System is finally connected to a Spectrum M2i4652 data acquisition card. For each individual point data is sampled for 5 s with a sampling frequency of 10 kHz.
To avoid uncertainties stemming from varying connections and mountings, for the velocity calibration of the hot-wire probes the traverse is moved into the highest position, which is well outside the laminar boundary layer and then different reference velocities are generated with the wind tunnel itself. The sampled voltage is then calibrated against the reference velocities using King's law.
The Dantec StreamlinePro system comes with a Thermistor based temperature probe to monitor the actual overheat ratio under varying flow temperatures. This temperature probe was mounted on the traverse arm. The StreamlinePro system readily converts the temperature into voltage, which is also sampled with the Spectrum M2i4652.

3.3. Traverse control

The traverse is controlled and operated with an Arduino Uno single-board micro-controller. The stepper motors are connected via standard stepper motor drivers and a laboratory type constant voltage supply. Fig. 9 shows the basic wiring diagram and names the exact driver types.
In a sense, the Arduino based traverse system is completely independent of the hot-wire and the data acquisition system.

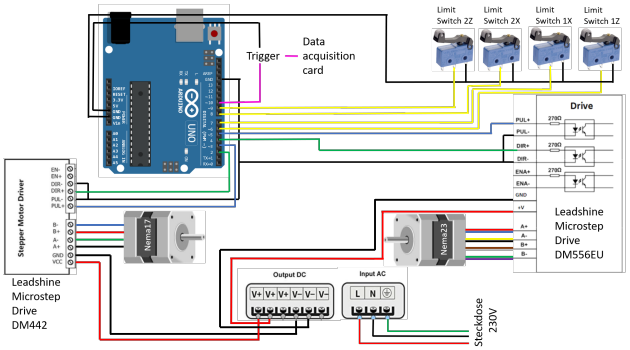

FIG 9. Wiring diagram of the hot-wire traverse

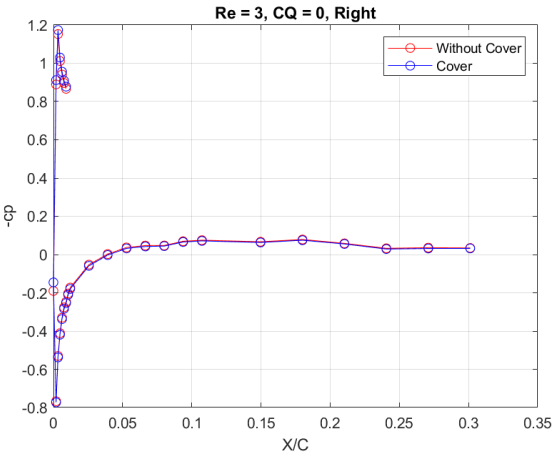

FIG 10. Measured pressure distribution at $Re = 3 \cdot 10^6$, with and without a sealing of the slits

However, a custom measurement code was written for the Arduino system to automatically loop through the different positions (i.e. to scan boundary layer profiles at different x/c). Whenever the traverse is stopping in a position ready for measurement, the Arduino Uno triggers to start the measurement on the Spectrum M2i4652 data acquisition card. This was done straightforward by connecting a digital output of the Arduino to one of the voltage inputs of the A/D-card and using a software-based rising edge trigger to start the data acquisition with the card.

4. RESULTS

The measured pressure distribution for the flat plate as used herein is shown in Fig. 10. Note that the stagnation point itself was not covered by a tap. The flow on the upper side of the plate accelerates smoothly to $c_p \approx -0.05$, whereas the flow on the lower side accelerates much more and reaches $c_p < -1$, which is however not relevant for the boundary layer on the upper side of the plate. Also note that the pressure distribution is shown here for $Re = 3 \cdot 10^6$, but is effectively independent of Re and also not influenced by the boundary layer suction.

Since the mechanical system of the traverse is finally larger than the thickness of the plate assembly, some slits had to be accepted on the lower side of the plate. This effectively creates an open connection between the two surfaces of the flat plate. To determine a possible influence on the boundary layers, the pressure was measured also with the bottom side slits being taped (which does not allow any operation of the traverse in this case). The pressure measurement in Fig. 10

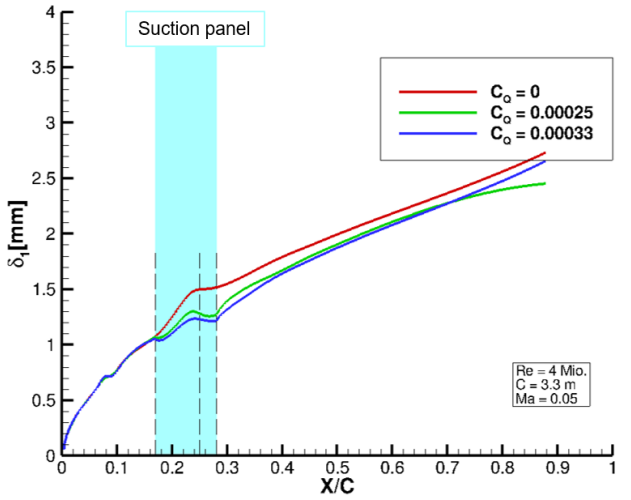

FIG 11. Displacement thickness along the flat plate at $Re = 4 \cdot 10^6$ for different suction rates, based on COCO

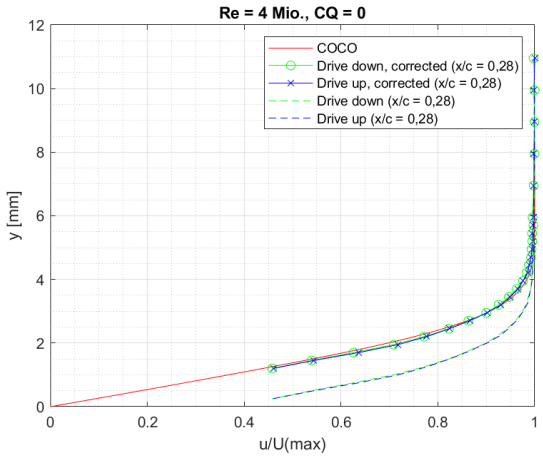

FIG 12. Measured and predicted boundary layer velocity profiles at the most downstream position, no suction

however shows that there is no notable impact of sealing the slits of the traverse. Therefore, for all subsequent measurements shown herein, the slits were left open. For later use, a small enclosure will probably be built to seal the underside of the panel.

The boundary layer prediction from COCO based on the measured pressure distribution is shown in Fig. 11 at $Re = 4 \cdot 10^6$ for different suction rates. The area, where suction can be applied, is highlighted in light blue. Three different positions along x where chosen here to measure boundary layer profiles, which are marked with a dashed line: $x/c = 0.17$, 0.24 and 0.28, where $x/c = 0.17$ is actually the leading edge of the suction panel and $x/c = 0.28$ is the trailing edge.

A result of a measured boundary layer velocity profile is shown in Fig. 12 along with the respective prediction from COCO. The measured data is shown here in two different ways: The raw data with the wall distance determined only from the position calibration is shown as a dashed line. As can be seen, the y-position of the raw data is off by some constant offset value. This offset value was determined and eliminated by fitting the measured velocity profile to the COCO result. Although this correction of the wall-normal position introduces a clearly unwanted coupling between the measured data and the predicted data, it is necessary

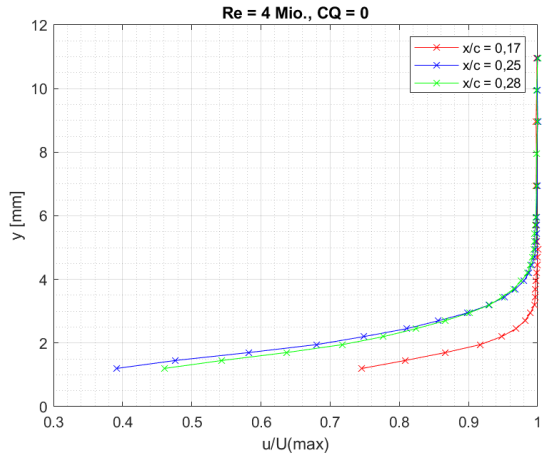

FIG 13. Boundary layer velocity profiles in three different positions on the suction panel (but without suction)

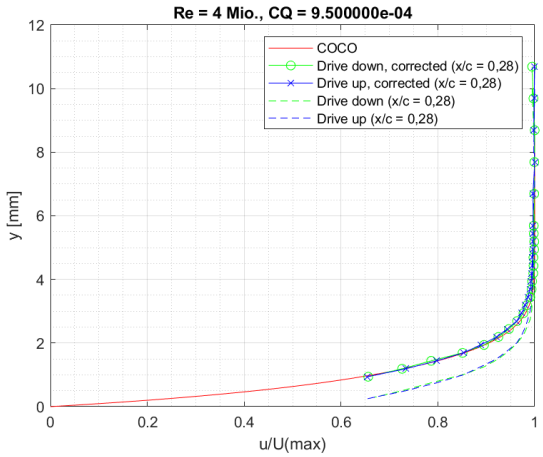

FIG 14. Measured and predicted boundary layer velocity profiles at the most downstream position with active suction

at the moment until an additional surface distance sensor can be implemented into the probe.

Once the y-position is corrected, the measured and the predicted velocity profiles agree very well. In this case the suction system was not operated (i.e. no net mass flow through the suction skin), but the micro-porous suction surface was otherwise left as-is. The excellent agreement between the COCO prediction and the measured velocity profile therefore shows, that a clean, but unused suction panels surface does not seem to have any significant influence on the boundary layer profile.

In Fig. 12 the measured profiles are also shown as "drive up" and "drive down" cases. This is since the traverse control program is currently only changing the x-position when the traverse arm is in the most extended position, i.e. at max y. The boundary layer profile is then measured once while the traverse drives downward and also while the traverse drives upward. As can be seen, the two profiles agree very well, which gives confidence that the accuracy of the traverse and the stationarity of the setup is good.

Fig. 13 shows the velocity profiles measured in the three positions for the same case. As generally expected, the boundary layer is much thinner at the leading edge of the suction panel, $x/c = 0.17$, than in the more downstream position. The two positions $x/c = 0.25$ and 0.28 are almost identical, which is also to be expected, since they are rather close to each other. It still highlights the repeatability of the probe measurements. The slight difference between the two profiles is basically in the region of the large velocity gradient. It may be the case that this difference is not physical, but a result of the y-position correction.

To show the effect of boundary layer suction, Fig. 14 shows the velocity profile in the most downstream position $x/c = 0.28$ for a case with relatively strong suction $c_q = 9.5 \cdot 10^{-4}$. The boundary layer is notably fuller and thinner than for the case without suction shown in Fig. 12. Still, the agreement between the COCO prediction and the measured velocity profile is very good. Note that, based on the measurements of Corelli Grappadelli et al. [10], the transition positions would be $x_{tr}/c \approx 0.48$ for $c_q = 0$, but $x_{tr}/c \approx 0.79$ for $c_q = 9.5 \cdot 10^{-4}$.

Fig. 15 shows the boundary layer profiles for a larger flow velocity than Fig. 14. The Re is twice as large, i.e. is $Re = 8 \cdot 10^6$ which causes the flow at $x/c = 0.28$ to be transitional or turbulent. For such case the measured velocity profiles are very different from the COCO prediction – the simple

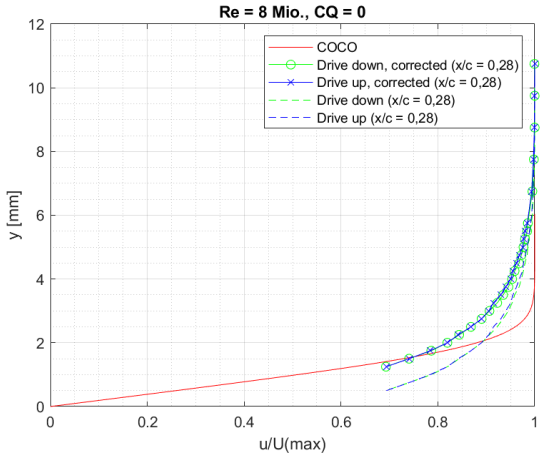

FIG 15. Measured and predicted boundary layer velocity profiles for a large $Re = 8 \cdot 10^6$ without suction

reason being, that COCO [16] is made to predict laminar boundary layers and does not have any turbulence modeling capabilities to also respect turbulent BLs. In such cases, since the COCO-prediction is clearly not akin the experimental data, also the correction of the wall-normal position is inaccurate.

The ultimate motivation to start the development of this hot-wire traverse for the flat-plat models, is to gain a better understanding of the development of the Tollmien-Schlichting instabilities, which cause the laminar-turbulent transition – particularly to acquire experimental data on damping rates for damped TS waves above suction panels.

Although this objective was not yet achieved, some preliminar data will be shown as an example in the following. The underlying test case is at $Re = 6 \cdot 10^6$. For this Re the flow is still laminar, as can be seen in Fig.16, but the amplitude of Tollmien-Schlichting modes (TS modes) is close to the stability limit. For the first test that will be shown herein, the suction is inactive so as to have the maximum amplitude. The development of the boundary layer thicknesses is similar as for the lower Re shown in Fig.13, due to the higher flow velocity, the boundary layer thicknesses are slightly reduced.

Fig.17 shows the corresponding N-factor curves predicted by LILO from the pressure distribution in Fig.10. For the experimental setup, a critical N-factor was calibrated by Corelli

et al. in previous work [10] and was found to be $N_{crit} \approx 8\text{-}9$, based on transition positions measured with infrared thermography. Note, however, that this was done during another experimental entry and flat plate experiments are known to be very sensitive, therefore the critical N-factor for this specific setup may differ from the previous calibration of Corelli et al. [10]. In any case, the exact value of N_{crit} is not so important at this point – is is more relevant to note that the local envelope N-factor at the position $x/c = 0.28$ is approximately $N \approx 7.6$ and the boundary layer shown in Fig.13 is clearly laminar. The N-factor curve highlighted in green belongs to the frequency of $483Hz$.

The boundary layer velocity data measured at $x/c = 0.28$, sampled at $10000s^{-1}$, was fourier-transformed and the amplitude distribution along y was derived from the fourier coefficients for fixed frequencies. In this specific case a frequency of $420Hz$ showed the largest amplitude near the wall, which is shown here as an example. Fig.18 shows the comparison between the amplitude functions predicted by LILO with a frequency of $483Hz$ and the amplitude function measured with the traverse, which is more pronounced for a frequency of $420Hz$. It can clearly be seen that the measured and the calculated amplitude functions are qualitatively similar.

In this specific case, however, other TS modes should have larger amplitudes than the $420Hz$ mode and this was not clearly seen in the measured data. Also it must be noted that the amplitude spectrum, i.e. the amplitude of the TS-modes per frequency, that was predicted by the stability theory, was not clearly found in the experiment. It is a matter of future work to tune the setup of the traverse, the CTA system and the data acquisition, and thus enable the system to measure more sensitive data.

5. SUMMARY

Primarily, the objectives of this study were to construct a hot-wire traverse, which is capable of moving in streamwise and wall normal directions on a flat plate to measure boundary layer velocity profiles in a wind tunnel experiment. This objective was achieved, the data were good enough to be compared with the computational results obtained using COCO and LILO. The measurements and the accompanying numerical simulations were carried out at Reynolds numbers from $Re = 3 \cdot 10^6$ to $Re = 8 \cdot 10^6$. In a post-processing step, the data were analyzed for instability modes, which were finally successfully obtained for both experimental and computational data. Despite having an offset error of the wall normal position in the measurement, all laminar boundary layer profiles that were measured in this paper agree very well with the COCO-predictions when the case is clearly laminar in the region of the probe. The influence of the boundary layer suction was also demonstrated. In cases where suction was active, significantly thinner boundary layer profiles are obtained. For cases that are either transitional or even turbulent ($Re > 6 \cdot 10^6$), the–yet necessary–correction of the wall-normal position based on COCO-predictions is not possible and therefore the wall-normal position becomes unreliable.

For future work with the hot-wire traverse, a method of measuring the absolute wall-normal position of the probe head in-situ for each measurement point, rather than relying on the stepper count, needs to be incorporated into the traverse.

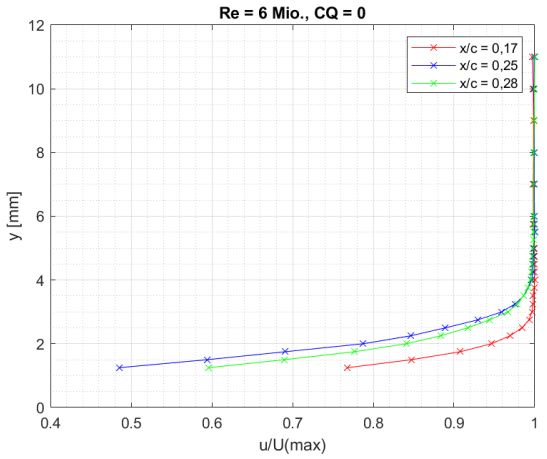

FIG 16. Boundary layer velocity profiles for the case $Re = 6 \cdot 10^6$ without suction

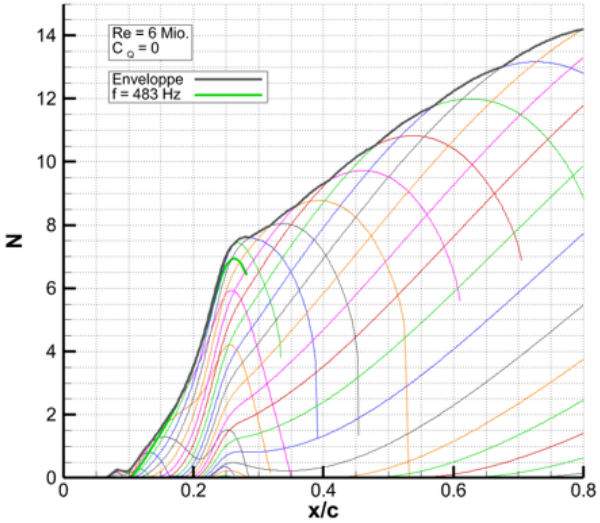

FIG 17. Stability properties, presented as N-factors, for $Re = 6 \cdot 10^6$ without suction

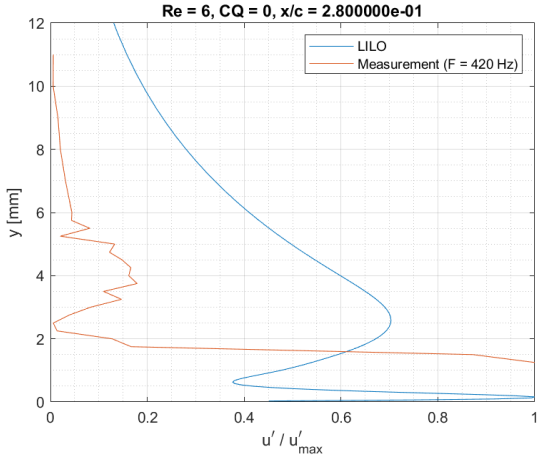

FIG 18. Measured and estimated amplitude function of the 420 Hz TS-wave at $x/c = 0.28$ (most downstream position)

ACKNOWLEDGEMENTS

The work is funded by the Deutsche Forschungsgemeinschaft (DFG) in the framework of the German Excellence Strategy in Cluster EXC 2163 "Sustainable and Energy Efficient Aviation" (SE²A) in ICA-B: "B1.5 - Sensitivities of Laminar Suction Boundary Layers for Large Reynolds Numbers". The authors deeply appreciate the contributions from JRG-B1 "Flow Physics of Laminar Wing and Fuselage" by Camli Badrya, Michelangelo Corelli Grappadelli, Rolf Radespiel in the development of the flat plate setup at MUB. We would also like to thank them for their cooperation and help in setting up the experiments presented herein.

References

[1] Ronald D Joslin. Aircraft Laminar Flow Control. *Annual Review of Fluid Mechanics*, 30:1–29, 1997. DOI: 10.1146/annurev.fluid.30.1.1.

[2] Nils Beck, Tim Landa, Arne Seitz, Loek Boermans, Yaolong Liu, and Rolf Radespiel. Drag Reduction by Laminar Flow Control. *Energies*, 11(1), Jan. 2018. ISSN: 1996-1073. Number: 1. DOI: 10.3390/en11010252.

[3] L.M.M. Boermans. Research on Sailplane Aerodynamics at Delft University of Technology. *Technical Soaring*, 30(1/2), January/April 2006.

[4] Anand Sudhi, Rolf Radespiel, and Camli Badrya. Design exploration of transonic airfoils for natural and hybrid laminar flow control applications. *Journal of Aircraft*, 60(3):716–732, 2023. DOI: 10.2514/1.C036968.

[5] K.S.G. Krishnan, O. Bertram, and O. Seibel. Review of hybrid laminar flow control systems. *Progress in Aerospace Sciences*, 93:24–52, 2017. ISSN: 0376-0421. DOI: https://doi.org/10.1016/j.paerosci.2017.05.005.

[6] Arne Seitz, Matthias Horn, Alexander Barklage, Peter Scholz, Camli Badrya, and Radespiel Rolf. Wind Tunnel Verification of Laminar Boundary Layer Control TSSD Concept. In *AIAA Aviation Forum 2022*, Chicago, USA, July 2022. AIAA 2022-3552. DOI: https://doi.org/10.2514/6.2022-3552.

[7] Heinrich Lüdeke and Christian Breitenstein. Experimental Investigation of Hybrid Laminar Flow Control by a Modular Flat Plate Model in the DNW-NWB. *CEAS Aeronautical Journal*, 13(1), January 2022. DOI: 10.1007/s13272-021-00564-0.

[8] Nathaniel Hilderbrand, Preethi V. Mysore, Meelan M. Choudhari, Balaji S. Venkatachari, and Pedro Paredes. Transition prediction of boundary layers in the presence of backward-facing steps. *AIAA Journal*, 60(7), April 2022. DOI: 10.2514/1.J061296.

[9] Heintz Alexander and Peter Scholz. Measurements on the Effect of Steps on the Transition of Laminar Boundary Layers. *Experiments in Fluids*, 64(4), March 2023. DOI: 10.1007/s00348-023-03614-x.

[10] Michelangelo Corelli Grappadelli, Stephan Sattler, Peter Scholz, Rolf Radespiel, and Camli Badrya. Experimental investigations of boundary layer transition on a flat plate with suction. In *AIAA SciTech 2021 Forum*, Virtual Event, January 2021. AIAA 2021-1452. DOI: 10.2514/6.2021-1452.

[11] Richard von Soldenhoff and Heinrich Lüdeke. Investigation of Interactions between Suction Chamber and Boundary Layer over Suction Walls using Direct Numerical Simulations. In *European Congress on Computational Methods in Applied Sciences and Engineering (ECCOMAS)*, Oslo, Norway, 2022.

[12] Alexander Barklage, Ulrich Römer, Arne Seitz, Matthias Horn, Rolf Radespiel, Peter Scholz, and Camli Badrya. Validation of suction velocity analysis for active laminar flow control with uncertainties. *AIAA Journal*, 61(9):3910–3922, 2023. DOI: 10.2514/1.J062374.

[13] Michelangelo Corelli Grappadelli, Paolo Olivucci, and Camli Badrya. Effects of boundary layer suction on a laminar separation bubble on a hlfc wing. In *AIAA AVIATION 2023 Forum*, San Diego, USA, June 2023. AIAA 2023-3955. DOI: 10.2514/6.2023-3955.

[14] Helge Koch, Peter Scholz, Reinhard Kerbstadt, and Martin Wermes. Eine autarke Sonde zur Messung von Grenzschichten im Flugversuch. In *Deutscher Luft- und Raumfahrtkongress 2015, DocumentID: 370211*, Rostock, Germany, 2015.

[15] Simon Schlüter. Auswertung von TSSD Absaug-Experimenten an einem modularen Plattenmodell im DNW-NWB. Studienarbeit, Deutsches Zentrum für Luft- und Raumfahrt (DLR), Technische Universität Braunschweig, Braunschweig, Germany, 2022.

[16] Geza Schrauf. Large-scale laminar flow tests evaluated with linear stability theory. *Journal of Aircraft*, 41(2), 2004.

[17] Geza Schrauf. LILO2.1 User's Guide and Tutorial. GSSC technical report 6, Bremen, Germany, 2004.

[18] Katharina Alt. Vermessung von Absaugegrenzschichten mit einer traversierenden Sonde. Studienarbeit, Technische Universität Braunschweig, Braunschweig, Germany, 2023.